# From Tomato Pomaces Biorefinery to Biobased Shape-Memory Semicrystalline Polyester Networks

Mathilde Marc, Christelle Lopez, Noemie Viller, Xavier Falourd, Mathieu Fanuel, Didier Marion, Eric Leroy, Benedicte Bakan, Denis Lourdin

# From tomato pomaces biorefinery to bio-based shape memory semi-crystalline polyester networks

Mathilde Marc†, Christelle Lopez†, Noemie Viller†, Xavier Falourd†‡, Mathieu Fanuel†‡, Didier Marion†, Eric Leroy[$], Bénédicte Bakan†*, Denis Lourdin†*.

† INRAE, UR BIA, F-44316, Nantes, France

‡PROBE research infrastructure, BIBS Facility, INRAE, F- 44316, Nantes, France

[$]Université de Nantes, Oniris, CNRS, GEPEA, UMR 6144, 44600, Saint Nazaire, France

*Corresponding authors

**Abstract**

The development of new bio-based polyester materials is of great interest. Seed-free and pulp-free peels provided by the biorefinery of industrial tomato wastes, i.e. pomaces, are rich in cutin, a polyester of hydroxy fatty acids. In this study, these fatty acids were recovered after alkaline hydrolysis resulting in a crude brown-colored extract, due to the co-extracted phenolic compounds. Further purification drastically reduces these phenolic compounds, resulting in a pale yellow product containing about 95% (9/10)-16-dihydroxy hexadecanoic acid and 5 % dicarboxylic fatty acids. Polymerization of the purified extract at 150°C results in a weakly crosslinked polyester network, with an estimated average number of 80 repeating units between nodes. Interestingly, the mechanical behavior of this material at 25°C is determined by its semi-crystalline structure. A necking phenomenon is observed during tensile tests resulting in an apparent plastic deformation of 286% and a Young modulus of 72 MPa. In addition, this bio-based polyester exhibits shape memory properties with the ability to be hot or cold- programmed. This work highlights the significant impact of minor compounds, related to the biochemical heterogeneity of agro-industrial waste products on the polyester properties and the potential of the biorefinery process to modulate the properties of biopolymers.

**Keywords**
hydroxy-fatty acids, phenolic, necking, bio-sourced, cutin-like

**Synopsis**.
Tuning the biorefinery of tomato pomaces enables the synthesis of a fully bio-based shape memory polyester material.

## Graphical abstract

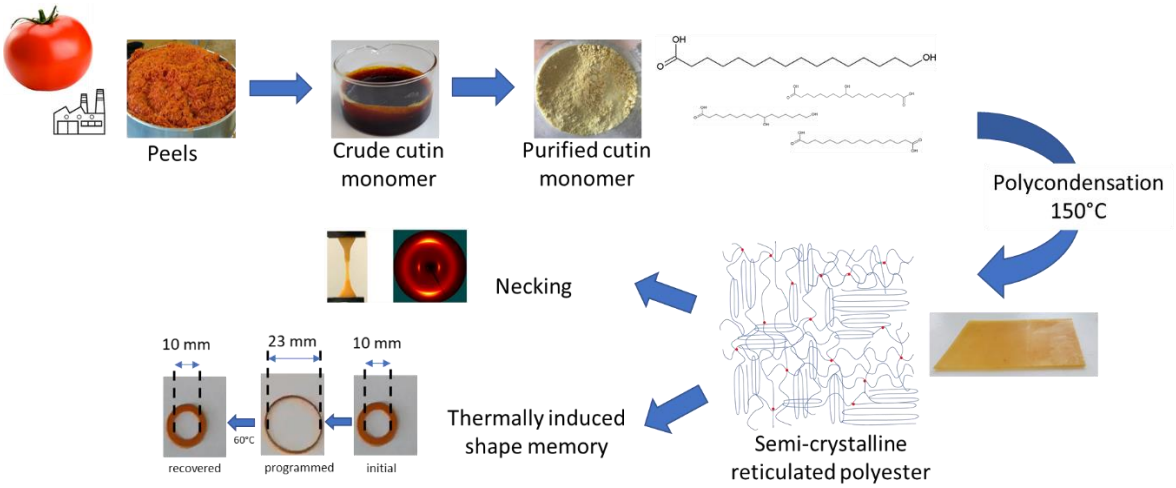


## Introduction

For both economic and environmental reasons, there is a great interest in new polyesters based on renewable carbon resources, without competing with food uses heredia[1, 2-4]. Intensive efforts are currently focused on the valorization of agricultural and food processing wastes as biorefinery feedstocks for the production of monomers [5-7]
Long-chain semi-crystalline polyesters with excellent mechanical properties [8, 9] can be produced from plant oils, with two major drawbacks: competition with food uses, and the need to chemically convert crude fatty acids into readily polymerizable monomers containing both hydroxyl and carboxylic groups [3, 8, 10]. Similar chemical structures, are naturally present in plant polyester i.e. suberin and cutin consisting in polyester network, biosynthesized from long-chain hydroxy fatty acids containing 16 to 18 carbon atoms [11, 12]. These monomers can be extracted from industrial by-products and can be used for polymer synthesis[7, 13-15] . However, the natural suberin composition is complex, which makes the control of the polyester functionalities more difficult. Conversely, tomato cuticle is rich in cutin polyester whose monomer composition is highly homogenous (tomato cutin mainly consists of 9(10)-16 hydroxy hexadecenoic acid). Tomato pomace is currently the largest and growing source of cutin-rich wastes [16], ranging from 6 to $9.10^6$ tons per year [17-19]. After separation from seeds and pulp, tomato peels, containing more than 60% cutin, can be hydrolyzed by alkali treatment, to yield fatty acid extracts containing mostly 9/10-16 dihydroxyhexadecanoic acid [7] with typically less than 10% of impurities such as α,ω-dicarboxylic fatty acids and phenolic compounds.

Several studies have shown that the thermal polymerization of such extracts leads to insoluble polyesters [7, 13, 16, 20-22] with a crosslinked structure. This indicates that the role of the minor compounds in the formation of the macromolecular structure should not be overlooked. Indeed, the polymerization of pure 9/10-16 dihydroxyhexadecanoic acid would be expected to lead to hyperbranched polymers [23] due to its ABB structure (A and B standing for acid and hydroxyl functions, respectively). While dicarboxylic fatty acids undoubtedly participate in thermal polyesterification, the exact role of phenolic compounds is probably more complex and difficult to control due to their high

reactivities [24]. In the present work, the amount of co-extracted phenolic compounds was greatly reduced by purification, with two objectives: i) to study the influence of dicarboxylic fatty acids alone on crosslinking, and ii) to get rid of the high coloring power of phenolic compounds, without resorting to chemical discoloration with hydrogen peroxide, with potentially detrimental effects on the polyester properties and human health, and thus on potential high value applications [4, 25].

Serendipitously this reduction of phenolic compounds leads to semi-crystalline crosslinked polyester with unusual mechanical behavior and shape memory properties. The relationships between this peculiar functionality and the thermal and structural properties of this new bio-based material are discussed.

## Materials and Methods

### *Material and chemicals*

Industrial tomato pomaces were provided by the "Conserveries de Bergerac" (UNIPROLEDI, Bergerac, France). Analytical grade solvents were obtained from Carlo Erba (Val de Reuil, France). Aminopropyl silica ($NH_2$) gel was purchased from Macherey-Nagel. Reference chemicals (gallic acid, p-coumaric acid, naringenin) were purchased from Sigma Aldrich (L'Isle d'Abeau Chesne, France).

## Methods

### *Cutin fatty acid monomers extraction and purification*

The crude cutin monomer (CM) fraction was extracted from peels isolated from industrial tomato pomaces according to the procedures previously described [7]. The crude dark brown colored CM extract was further purified by aminopropyl silica column chromatography according to a modification of a described procedure [26]. The aminopropyl silica (100 g) dispersed in chloroform:2-propanol 2:1 (v:v) was poured into a glass column (50 cm x 5 cm) with a fritted glass filter and a Teflon tap placed on the bottom. The crude cutin monomer extract (10g) solubilized in the chloroform:isopropanol mixture (50mL) was applied to the aminopropyl phase. After elution with 1L of the chloroform:isopropanol mixture, the hydroxy fatty acids were eluted with 1.5L of chloroform. After evaporation of the solvent under vacuum and further thorough freeze-drying, the pale yellow solid was recovered and stored in a dark place at room temperature. Four purification batches were pooled to perform the experiments. The depigmented hydroxy-fatty acid fraction was further referred as "purified CM" fraction. Total phenolic content was determined by the Folin-Ciocalteu colorimetric assay [27] using gallic acid for the standard curve. It was expressed as mg of gallic acid equivalents (GAE)/g cutin monomer extract. In addition, the phenolics profile was performed by a high-performance liquid chromatography (HPLC)-diode array detection (DAD) method [28] on an Acquity ARC system (Waters, USA) with a diode array detector, using a BEH X-Bridge C18 column (250 × 4.6 mm, 5 µm) and guard column (20 × 4.6 mm, 5 µm).

The fatty acid composition was determined as previously described by GC-FID-MS [29] and matrix-assisted laser desorption/ionization (MALDI)-time-of-flight (TOF) MS adapted from [30]. A DHB (2,5-dihydroxybenzoic acid) solution at 3 $mg.mL^{-1}$ in H2O/methanol (1:3) with 2.5 mM of LiCl was used as the MALDI matrix. The samples were mixed with the matrix solution in a 1:9 ratio (v/v) and the mixture (1 µL) was deposited on a polished steel MALDI target plate. MALDI measurements were then

107 performed on a rapifleX MALDI-TOF spectrometer (Bruker Daltonics, Bremen, Germany) equipped
108 with a Smartbeam 3D laser (355 nm, 10000 Hz) and controlled using the Flex Control 4.0 software
109 package. The mass spectrometer was operated with positive polarity in reflectron mode. Spectra were
110 acquired in the range of 180–5000 m/z. Chemical labelling of the free OH by benzyl-etherification was
111 performed as previously described [31].

112 The monomeric content of the hydroxy fatty acid fractions was determined by size-exclusion
113 chromatography on a Waters HPLC system coupled to an evaporative light scattering detector (Sedere
114 Sedex 75 ELSD, Alfortville, France). A home-packed column (30 cm X 1 cm) of Sephadex ® LH20 l(Sigma-
115 Aldrich) was used and elution with methanol was performed at 1mL.min$^{-1}$25°C with methanol. PEG
116 standards were used for molecular mass calibration.
117
118 ***Polyester synthesis and characterization***

119 Several films of typically 700 ± 50 μm thickness was produced by bulk poly-condensation as
120 previously described [7]. Briefly, an amount of purified CM was put in Teflon molds (5cm × 5cm or 10cm
121 x 10 cm) and baked for 24h at 150°C in an oven. Vacuum was applied during the first 120 min. to avoid
122 the formation of bubbles. This also facilitated the removal of the water molecules generated by the
123 polyesterification. Then, the water molecules vaporizated by heating at high temperature were
124 trapped in a beaker containing dry silica gel. These films were characterized using the techniques
125 described below. Mechanical tests were only possible on 10 cm x 10 cm films. Shape memory was
126 qualitatively tested on all films.

127 Attenuated total reflectance Fourier-transform infrared spectroscopy (ATR-FTIR) spectra were
128 recorded on a Nicolet Magna IR 550 spectrometer (Thermo Fisher Scientific, Saint-Herblain, France)
129 equipped with a liquid nitrogen-cooled mercury–cadmium–telluride detector. The instrument was
130 continuously purged with dry air. Spectra of polyester films were obtained by attenuated total
131 reflection (ATR) using a single reflection accessory equipped with a diamond crystal at a 45° angle of
132 light incidence. All spectra (3 per polyester) were acquired in the 4000 to 700 cm$^{-1}$ range with a
133 resolution of 2 cm$^{-1}$ and accumulation of 30 scans. Spectral deconvolution was performed using Fytik
134 software[32] .

135 $^{13}$C solid-state NMR (SSNMR) was performed on a Bruker AvanceIII-400 MHz spectrometer
136 operating at 100.61 MHz for $^{13}$C, equipped with a double-resonance H/X CP-MAS 4-mm probe (Bruker
137 Biospin, Wissembourg, France). A cross-polarization magic-angle-spinning experiment (CP-MAS) was
138 performed. Briefly, 80 mg of the co-polyester films were packed into 4 mm zirconia rotors. The samples
139 were spun at 12,000 Hz at room temperature. The CP-MAS spectrum was acquired with a contact time
140 of 1.5 ms, a recycling delay of 8 s and an accumulation of 8192 scans. The carbonyl carbon was set to
141 176.03 ppm through external glycine calibration. Spectral deconvolutions were performed using
142 PeakFit® software (Systat Software, Inc., USA).
143
144 ***Rheology during polymerization***

145 Crude and purified CM samples were placed in a dynamic rotational rheometer (HAAKE MARS
146 III). A plate–plate geometry (diameter 20mm, gap 1mm) was used. The rheometer was preheated at
147 150°C before the samples were introduced and a 0.01% sinusoidal deformation was applied at 1Hz.
148 The evolution of moduli G' and G'' resulting from the thermal polymerization at 150°C was thus

monitored. Note that unlike the polymer synthesis conditions, vacuum could not be applied during the first 120 minutes of the reaction in the rheometer. In addition, the free surface area at the edge of the material between the plates is significantly smaller than that of the samples polymerized in the oven. Therefore, the water molecules formed by the polyesterification reaction are expected to take more time to diffuse and escape into the air surrounding the material.

***Differential Scanning Calorimetry***

Differential Scanning Calorimetry (DSC) measurements were performed with a DSC Q100 (TA Instruments, Newcastle, DE). The calorimeter was calibrated with indium (ΔH = 28.41 $J.g^{-1}$; melting point of 156.66°C). A piece of polyester (weight about 8 mg) was loaded into a hermetically sealed aluminum pan. An empty and hermetically sealed aluminum pan was used as reference. The DSC pans were introduced in the calorimeter at 20°C. The scanning rate was 3°$C.min^{-1}$, or 5°$C.min^{-1}$ to be in similar conditions as for XRD measurements as a function of temperature. Data analysis was performed using TA Universal Analysis program. The melting transition temperature (Tm) was taken at the peak maximum recorded during heating. Enthalpy changes of the transitions (ΔHm) were obtained from the area under the peak. The DSC experiments were performed in triplicate, by preparing and analyzing three independent pans.

***X-ray diffraction***

X-ray diffraction (XRD) measurements as a function of temperature were performed on the high brilliance SWING beam line at the SOLEIL synchrotron facility, with the monochromator set at 12 KeV. Using a EIGERX 4M detector at a distance of 0.519 m from the sample, diffraction patterns were recorded for reciprocal spacing q. The q range allowed the characterization of the packing of the acyl chains of the polyester. 1D XRD curves were obtained by circular averaging of the 2D images using the Foxtrot software. A piece of polyester was loaded into thin quartz capillaries of 1.5 mm diameter (GLAS W. Muller, Berlin, Germany). The capillary was inserted into a Linkam oven (Linkam Scientific Instruments Ltd, Waterfield, UK). This set-up allowed synchrotron-radiation XRD as a function of temperature. The XRD experiments were conducted at fixed temperature (20°C) and on heating from 20°C to 95°C at 5°$C.min^{-1}$ (375 patterns; 1 frame each 0.2°C; 0.5 sec exposure time and 0.5 sec gap time). The three-dimensional plot of the XRD patterns as a function of temperature was generated using R software (R Foundation for Statistical Computing, Vienna, Austria). PeakFit software (Jandel Scientific, Germany) was used to determine the positions of the Bragg reflections.

For crystal orientation studies, two-dimensional wide-angle X-ray scattering (WAXS) diagrams were recorded using a Bruker D8 X-ray diffractometer (Madison, WI) equipped with a two-dimensional GADDS detector. The X-ray radiation, Cu KR1 (λ = 0.154 05 nm), produced in a sealed tube at 50 kV and 1 mA was selected and parallelized using a Gobel mirror parallel optics system and collimated to produce a beam diameter of 500 µm. WAXS diagrams were recorded in the transmission mode with the specimens lying with their length parallel to the vertical axis of the detector. Orientation was determined by azimuthal integration between 0.680 and 0.386 nm corresponding to the amorphous scattering band. Background and beamstop profiles were subtracted from the sample signals; the resulting signal was smoothed for more clarity. The acquisition time was 15 min.

***Dynamic mechanical thermal analysis***

189 Dynamic mechanical thermal analysis (DMTA) was performed on a DMTA MKIV (Rheometric
190 Scientific, US). Rectangular specimens (20 mm × 4 mm) were cut from the films and the thickness of
191 about 0.7-1 mm was accurately measured with a micrometer. The samples were analyzed in the tensile
192 mode at the frequency of 1 Hz with a strain amplitude of 0.1 %. To keep the samples taut, a static force
193 was applied to the sample that was 10% higher than the dynamic force. A scanning rate of 3 °C·min$^{-1}$
194 from -50 °C to 80 °C was used. Each sample was analyzed in duplicate. For recovery measurements, a
195 very weak static force of $10^{-3}$N is applied to the sample in order to follow the free shrinkage of the
196 sample during its heating.

197 ***Mechanical properties***

198 Tensile testing of the films was performed using the MTS Synergie 100 (MTS Systems
199 Corporation, USA). The film samples were cut into a dog-bone shape and their thickness were
200 accurately measured with a vernier caliper. The test was performed using a cross-head speed of 10
201 mm/min. The reported results, including Young's modulus, ultimate strength, and elongation at break,
202 were the average values of five specimens.

203

204 **Results and Discussion**

205 ***Cutin monomer purification impacts the polymerization process***

206 The purified tomato CM extracts mainly consist of hydroxy fatty acids as evidenced by FT-IR
207 spectra dominated by intense stretching vibrations of the methylene chains (asymmetric ($CH_2$) and
208 symmetric ($CH_2$) at 2919 cm$^{-1}$, and 2850 cm$^{-1}$ respectively, bending $CH_2$ at 722 cm$^{-1}$) and a sharp band
209 at 1704 cm$^{-1}$ assigned to carbonyl stretch of carboxylic group. A broad hydroxyl (3300–3500 cm$^{-1}$) band
210 was also observed. In addition, chemical analysis (Figure 1A) highlighted that the CM extracts
211 concentrated more than 90% of 9 -and 10,16 dihydroxyhexadecanoic acid isomers, (hereafter designed
212 as diOHC16), as well as 1.5% of the 16-hydroxyhexadecanoic acid and 5% of the dicarboxylic fatty acids
213 (10-hydroxyhexadecanedioic acid and hexadecanedioic acid). The purification step led to the reduction
214 of several phenolic specific bands in the FT-IR spectra at 1626 cm$^{-1}$ (stretching of conjugated C=C in
215 aromatics), 1606 cm$^{-1}$ (stretching band (C-C) aromatic), 1515 cm$^{-1}$ (stretching of C-C aromatic
216 conjugated with C=C) and 833 cm$^{-1}$ (out of plane bending of (C-H) aromatic). Likewise, biochemical
217 analyses (Figure 1B) indicated a nearly 10-fold reduction from 45 mg/g (GAE) to 5 mg/g (GAE) while
218 the fatty acid composition remains almost unchanged. Regarding the lab-scale process to reduce the
219 phenolic content of the crude CM extract, some improvements can be made by replacing the non-
220 green and hazardous chloroform by the eco-friendly solvents, cyclopentyl methyl ether (CPME; De
221 Gonzalo et al, 2019) and acetone (supplemental data Figure 1). However, it should be emphasized that,
222 regardless of the solvent, this costly purification process cannot be up-scaled from an industrial
223 perspective. Indeed, the main phenolic fraction, consisting of the corresponding oxidized compounds,
224 is irreversibly bound to the aminopropyl silica gel and cannot be reused. Actually, the lab-scale process
225 was used as a proof-of-concept to highlight the effects and benefits of reducing the phenolic content
226 of the crude CM extracts of tomato pomaces.

227

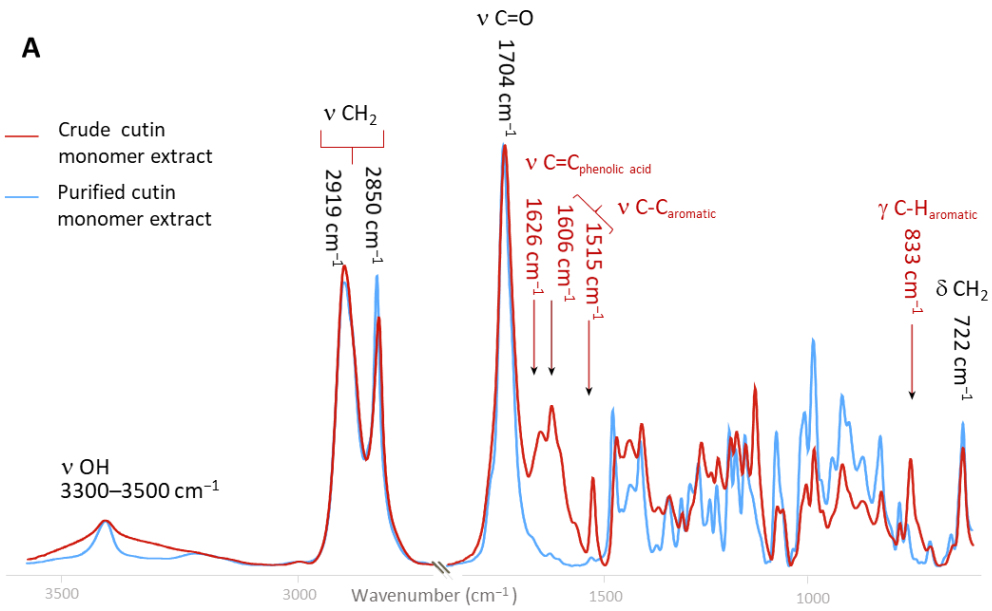


**B**

| Cutin monomer extract | crude | purified |
|---|---|---|
| a 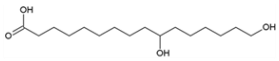 | 94 % | 93 % |
| b 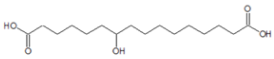 | 3,7 % | 4.5 % |
| c 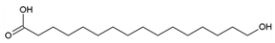 | 1,9 % | 1.5 % |
| d 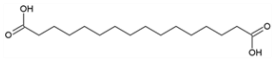 | 0.4 % | 0.5 % |

228

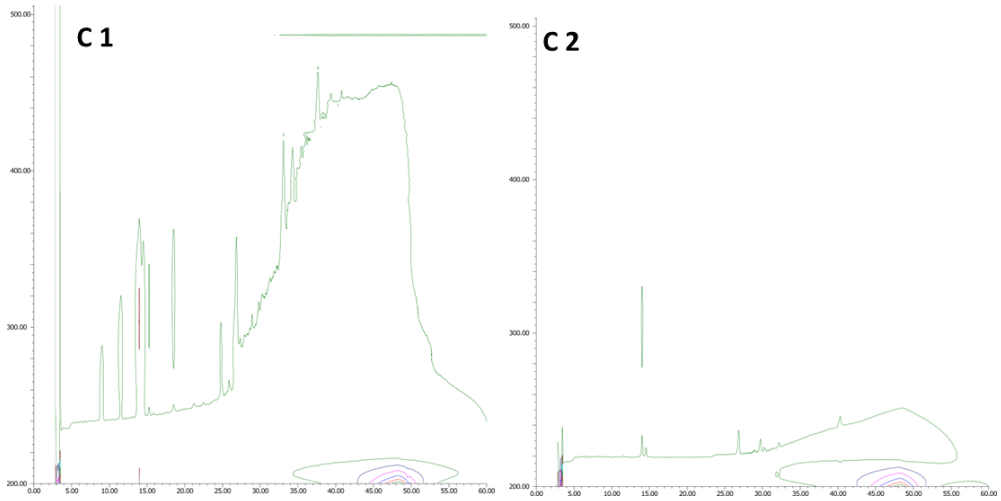


229 Figure 1: (A) FT-IR characterization of the cutin monomer extracts before and after purification. (B)
230 Lipid composition (% of fatty acids) of the cutin monomers before and after purification a: 9,10-16
231 dihydroxyhexadecanoic acid; b: 10-hydroxyhexadecanedioic acid; c: 16-hydroxyhexadecanoic acid; d:
232 hexadecanedioic acid. (C) Total phenolic compounds were determined by Folin Calieu analysis (inset-
233 data expressed as mg of equivalent gallic acid per g of cutin extract) and monitored by HPLC-DAD.
234 Contour plot of the crude cutin monomer extract (C1) and CPME-purified cutin monomer (C2).

Thermal polycondensation resulted in a light-brown solid material insoluble in water and chloroform. Assuming that the contribution of the traces of phenolic compounds present in the purified CM fraction to the polymerization can be neglected, only the fatty acid building blocks are involved in the reaction. The results of the rheological tests show a strong impact of the purification on network formation kinetics during polymerization. Figure 2 shows the evolution of the G' and G'' moduli monitored during isothermal polycondensation at 150°C for the purified and crude CM fractions. Initially, both samples display a viscous liquid behavior (G'' >> G'). However, gelation phenomena take place during the reactions, leading to a viscoelastic solid behavior (G' > G''). The modulus crossover time (G' = G'') gives a rough estimate of the gel time, which is likely to be shorter during the oven polymerization of films both because of the presence of vacuum at the beginning, and the larger free surface area, which favors the removal of the water molecules formed during the polyesterification reaction, thus accelerating it. However, while the modulus crossover occurs at ≈ 2.2h for the crude fraction, it is observed after 9h for the purified one, which represents a 4-fold increase. Such a huge difference suggests that the gelation times which are thought to be shorter during the oven polymerization experiments, are still very different. Therefore, the following conclusions can be drawn: i) The presence of gelation phenomena for purified CM demonstrates that the mere presence of 5% dicarboxylic acids is sufficient to lead to a crosslinked polyester network by co-polymerization with the main diOHC16 fatty acid component ii) The approximately 4-fold shorter gelation time observed for the CM extract suggests that the presence of phenolic compounds participates in side reactions inducing additional crosslinking. Therefore, it was decided to further focus on the polyester obtained from the purified CM fraction.

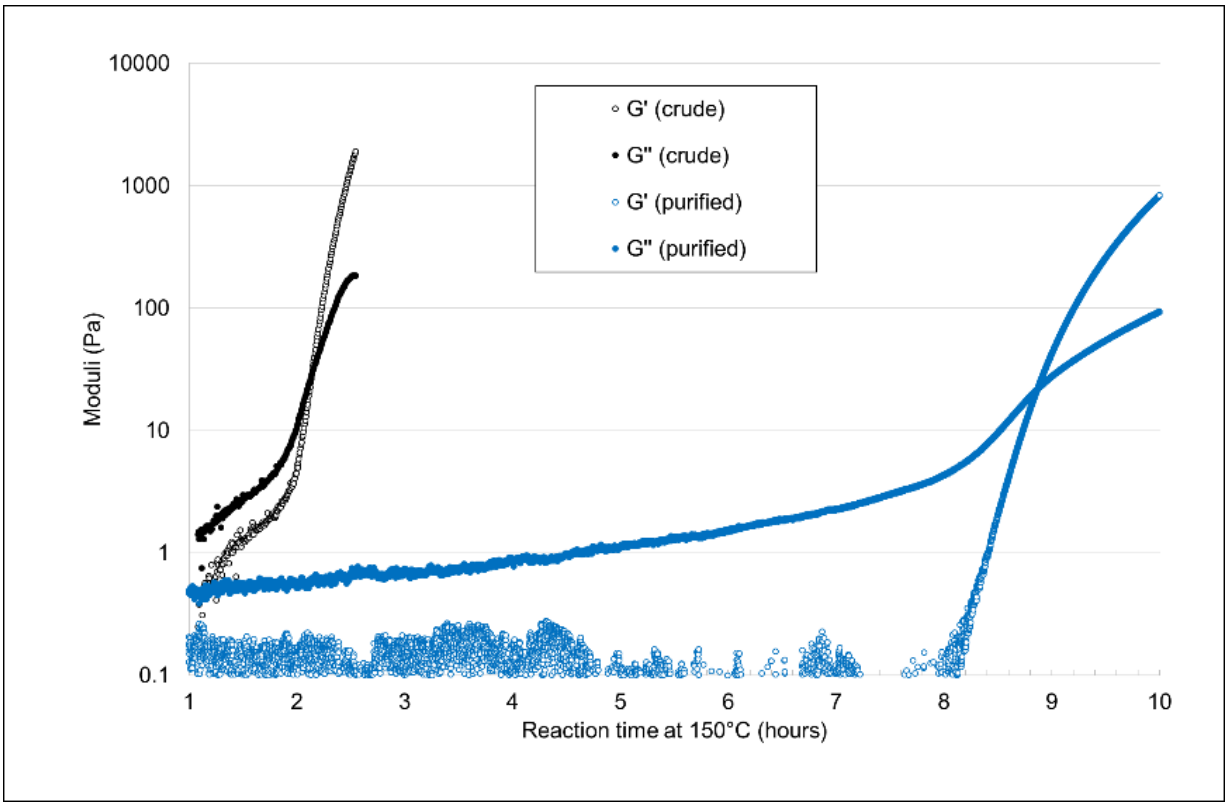


Figure 2: Evolution of the moduli G' and G'' during polymerization at 150°C for the crude and purified CM fractions.

***Ester and hydrogen bonds govern the polymer structure***

The structure of the polymer determined by ATR-FTIR and $^{13}C$ SSNMR (Figure 3) highlighted typical polyester features. Indeed, the FTIR spectrum showed the characteristic shift of the carbonyl band from 1704 $cm^{-1}$ (Figure 1A), assigned to the carboxylic acid of the monomers, to the band around 1730 $cm^{-1}$ assigned to the carbonyl ester stretching vibration ($\nu_s$ C=O) (Figure 3A)[33] . The polymer also displayed C-O-C ester stretching bands (1166 and 1106 $cm^{-1}$ respectively). The $\nu_s$ C=O band can be deconvoluted into two bands at 1731 and 1715 $cm^{-1}$. The latter is generally assigned to carbonyl involved in hydrogen bonds (H-bonds) with an hydroxyl group while the former is considered to be free carbonyl group, i.e., not involved in hydrogen bonds[34] . This band splitting has also been observed in plant cuticles [29, 33]. In cuticles this lowest wavelength $\nu_s$ C=O band is attributed to interactions of the cutin polyester with cuticle-embedded polysaccharides and non-esterified hydroxy fatty acids. In this study, the H-bonds can only involve the non-esterified hydroxyl group of the hydroxy-fatty acid monomer units of the polyester. The vibration at 1715 $cm^{-1}$ is broader than the band at 1733 $cm^{-1}$ indicating a relatively wide distribution of hydrogen bond distances and geometries in the polyester. The H-bonds can also be observed in the large OH stretching vibrations in the 3000-3500 $cm^{-1}$ region. Four major peaks can be highlighted after deconvolution, i.e. at 3204, 3331, 3431 and 3505 $cm^{-1}$ (Figure 3) in agreement with previous results on hyperbranched polyester polyol [35]. These different deconvoluted peaks can be attributed to different types of hydrogen bonding between C=O and OH groups (C=O:::H-O) and between OH groups (O-H:::O-H) [36, 37]. The three deconvoluted peaks at 3204, 3331, 3431 $cm^{-1}$ are due H-bonding of different strengths, i.e., the lowest OH wavelength is related to the strongest H-bonding.

Similarly, $^{13}C$ SSNMR show a broad peak at 172.6 ppm assigned to esterified carbonyl (Figure 3B) and a sharp peak at 64 ppm, which is assigned to primary esters [22]. The presence of a smaller peak at 61.8 ppm indicates non-esterified primary hydroxyl group. Spectral deconvolution allowed us to estimate at 72 ±1% the proportion of esterified chains. According to the chemical structure of the diOHC16 including mid-chain and ω-hydroxyl groups, both, linear and branched ester bonds, can be formed in the polyesters. The esterification scheme of the polyester was further monitored by the chemical labeling of the free OH groups within the diOHC16-derived polyesters [31]. After complete depolymerization, the release of diOHC16 containing labeled OH groups either in ω-position or in the midchain-position was compared (Figure 3C). Within these labeled monomers, the relative proportion of labeled mid-chain OH/ ω-OH labeled in diOHC16 indicated that the free OH groups were mostly (84%) in the mid-chain position. This indicates that the two OH groups of the ABB monomer do not have the same reactivity, favoring the formation of “head to tail” linear sequences and limiting the formation of side pendant chains.

Finally, the polymer was subjected to alkaline hydrolysis. The product obtained after alkaline hydrolysis display the same fatty acid monomer composition (Supplemental Figure 2A) and its size distribution superimposed on that of the purified CM fraction (Supplemental Figure 2B), indicating the presence of ester linkages in the polymer. This ester structure is an advantage for the recyclability of this bio-based polymer.

All these data indicate that the structure of the polymer is controlled by both ester and hydrogen bonds. The polyester contains both linear and branched polymer chains of different masses with a preferential linear polymerization scheme. Since the polyester is reticulated, the minor dicarboxylic fatty acids (Figure 1B) are most likely involved in the polymer cross-linking.

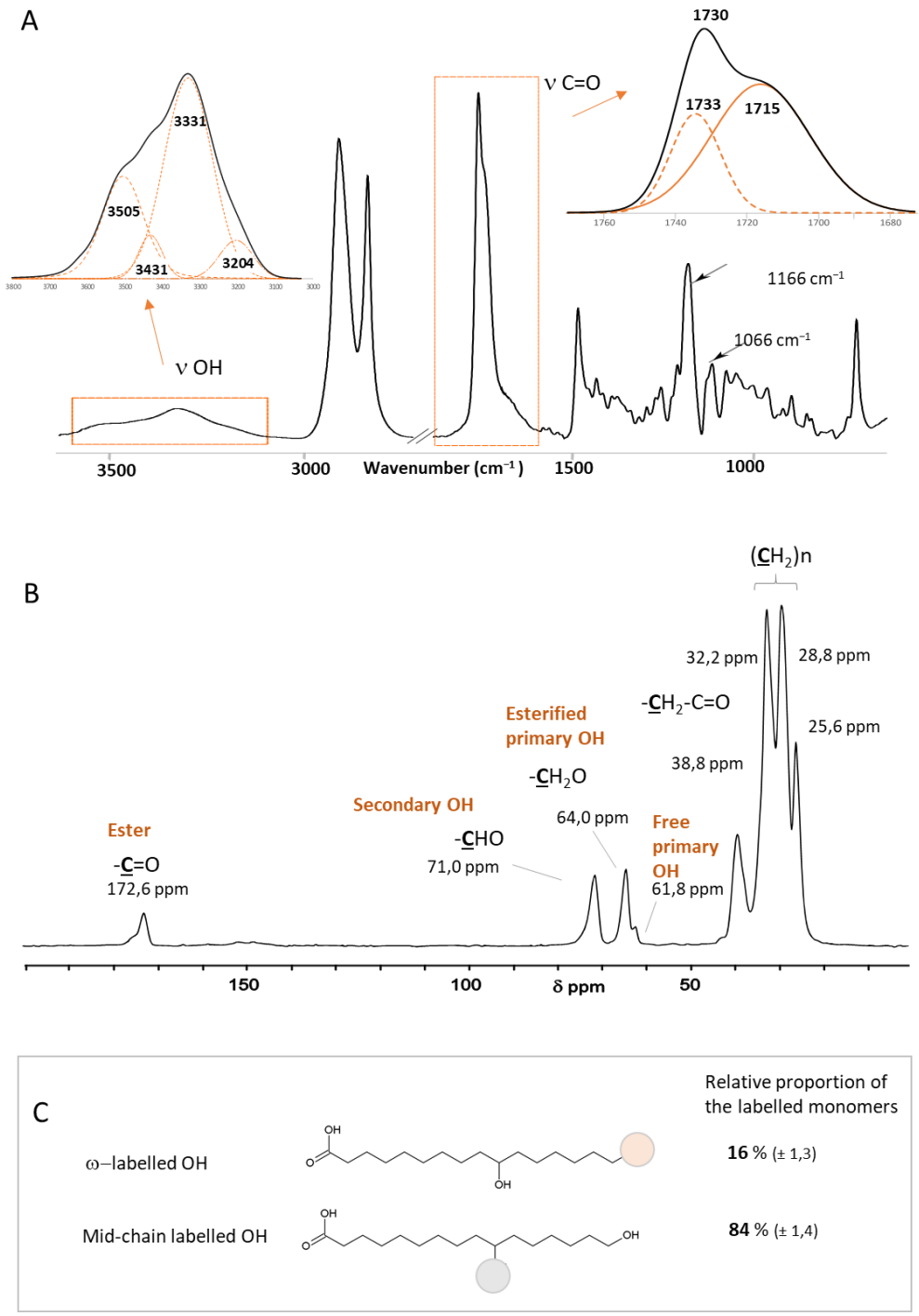


Figure 3 : (A) ATR FTIR spectra of polymer produced from the purified cutin monomer. Typical polyester bands (arrows) were observed at 1730 $cm^{-1}$ ( streching of esterified C=O), 1166 $cm^{-1}$ (asym streching of the C-O-C ester bound) and 1106 $cm^{-1}$ (symetric streching of the C-O-C ester bounds). In inset, a magnification of the OH streching bands involved in different hydrogen bond and of the CO streching bands at 1730 and 1715 $cm^{-1}$ assigned respectively to ester group and ester group involved in hydrogen bond. (B) Solid state $^{13}C$ CP-MAS spectrum of the polyester. (C) Inset- Relative proportion of free OH groups within the polyester at the ω- and mid-chain position of the the diOHC16. Values are means of at least three replicates (± standard deviation).

313 ***Thermal transitions highlight the semi-crystalline structure and the network of the polyester***

314 Figure 4 shows the thermograms obtained by DSC on a first heating of the polyester, on the
315 cooling immediately followed by a second heating. At low temperatures, the thermogram show a glass
316 transition (Tg) at -25°C, which is determined at the midpoint of the baseline fall. At higher
317 temperatures, the thermogram of the first scan shows a large melting endotherm beginning at about
318 38°C and with a maximum at 51.2°C. Above 60°C the transition appears to continue slowly and the
319 baseline recovers at about 80°C. On cooling, the DSC thermogram shows an exotherm with a maximum
320 at 30.0°C, attributed to the crystallization of the polyester chains. The second heating obtained after
321 cooling shows a broader melting endotherm that seems to start at around 10°C. These results suggest
322 an aging during the storage of the polymer which allows crystallization. This is confirmed by a melting
323 enthalpy of 61.8 J/g for the first heating and 41.1 J/g for the second heating. In order to « standardize »
324 the conditions of the study, the calorimetric, mechanical and thermomechanical experiments were
325 carried out on samples stored for 7 days at 20°C after heating above the melting temperature. The
326 thermal stability was studied by thermogravimetric analysis (supplemental Figure 3). A very low weight
327 loss (less than 0.5%) below 100°C probably corresponds to moisture evaporation. Thermal degradation
328 occurs above 300°C which is similar to other bio-sourced polyesters such as PBS. According to the
329 calorimetric results, we further investigated the structure of the crystal domains by X-ray diffraction.

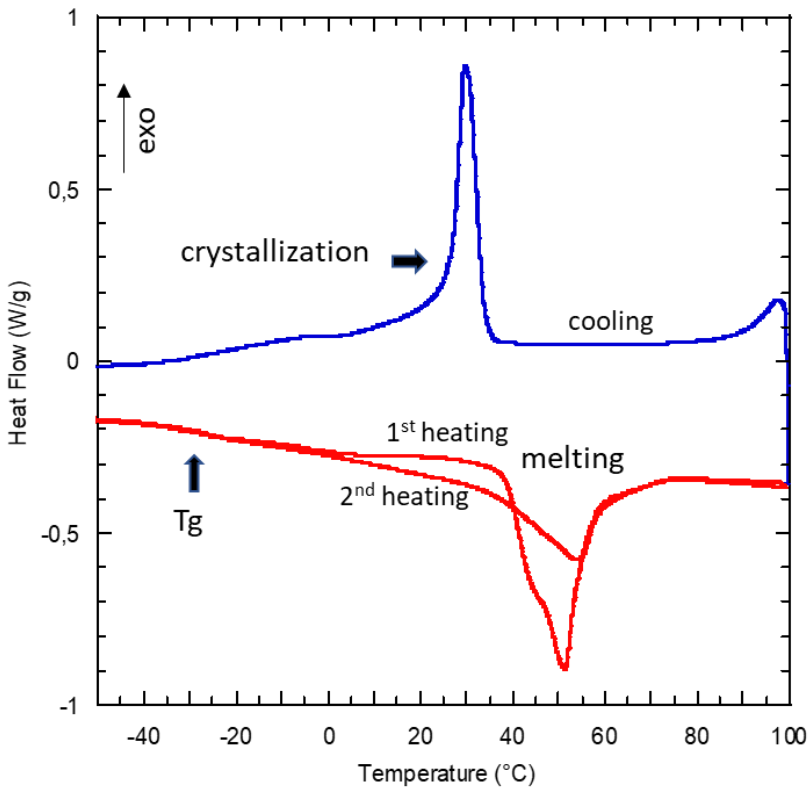


330

331 Figure 4: Thermograms obtained by DSC on a first melting, cooling and second melting of the polyester.

332 The XRD patterns recorded at 20°C revealed that the polyester exhibited a crystalline phase
333 with a lateral packing of the chains in the orthorhombic sub-cell (β' polymorphic form), characterized
334 by two peaks at 1.4900 and 1.5977 $Å^{-1}$ (4.2 and 3.9 Å, respectively) (figure 5A). A peak was recorded at
335 0.6208 $Å^{-1}$ (10.1 Å). Since the carbon–carbon distance in an aliphatic chain is 1.27 Å [38], the chain length

of an acyl chain containing 16 carbon atoms, such as the diOHC16 molecules, was calculated to be 19.05 Å. The peak at about 10 Å was interpreted as a longitudinal organization of the chains with a repeat distance corresponding to the half chain length of the acyl chains of diOHC16 in the crystallized state. On heating of the polyester at 5°C.min$^{-1}$, the diffraction peaks corresponding to both the lateral packing and the longitudinal organization of the chains, progressively decreased in intensity between about 40°C and 60°C. This was interpreted as the melting of the acyl chains as a function of the increase in temperature. For temperatures above 60°C, the bump of X-ray diffusion centered at 1.3694 Å$^{-1}$ (4.58 Å) was attributed to the acyl chains in their molten state, in agreement with the literature [38]. The DSC thermogram recorded at the same heating rate (figure 5B) showed a broad endotherm with Tm = 59.7 ± 0.5°C, and ΔHm = 73.9 ± 1.9 J.g$^{-1}$ polyester (means calculated from 3 independent samples). This endotherm was similar to the endotherm recorded in the temperature range from -50 to 100°C (figure 4). After rapid cooling of the polyester from the melt (95°C), the wide-angle XRD signal revealed the formation of an hexagonal packing of the acyl chains ($\alpha$ polymorphic form) characterized by a single peak at q = 1.4926 Å$^{-1}$ (d = 4.2 Å), and a longitudinal organization (d = 10.5 Å). At 20°C, the freshly melted polyester was in a hexagonal packing ($\alpha$ polymorphic form) while the « aged » sample, after 7 days at room temperature was in an orthorhombic $\beta$' polymorphic form. Differences in the packing of the chains as a function of the thermal history of the polyester revealed a polymorphism with a variable metastability of the crystallization state (figure 5C). Regardless of the aging of the samples and the polymorphic form of the crystallized acyl chains, the peak at about 10 Å corresponding to the longitudinal organization of the chains was recorded at 20°C.

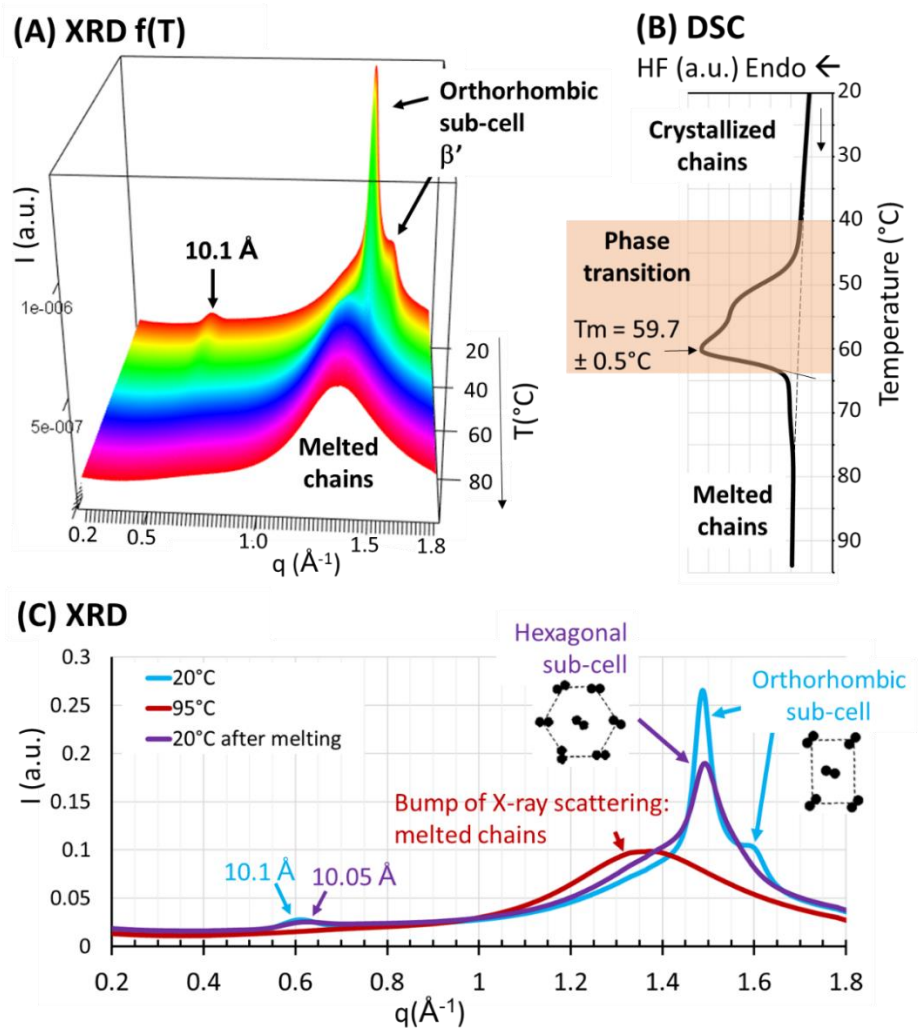


Figure 5: (A) 3-dimensional representation of XRD patterns recorded as a function of temperature on heating of the polyester from 20°C to 95°C at 5°C.min$^{-1}$ ; (B) Thermogram recorded on heating of the polyester from 20°C to 95°C at 5°C.min$^{-1}$ ; (C) XRD patterns recorded at various temperatures as indicated in the figure.

The characterization of dynamic properties by DMTA has been realized in order to investigate the amorphous state. Figure 6 shows thermomechanical storage (E') and loss (E'') moduli, measured by DMTA. At low temperature, the storage modulus of the material was typical of a glassy state (E' ≈ 1 GPa at -50°C). Its first drop between -40°C and 0°C, coinciding with the E'' peak centered around -20°C corresponds to the main mechanical α-relaxation associated with the calorimetric glass transition from glassy to rubbery state determined by DSC (figure 4). The storage modulus value obtained above this transition is maintained at a rather high value (E'≈ 100 MPa at 20°C) due to the presence of the crystalline fraction previously shown. The thermomechanical measurements showed a dramatic second drop in the moduli starting from about 45°C, due to the melting of this crystalline part of the material, leading to a plateau in the storage modulus. Its average value of E' ≈ 0.4 MPa at 70°C, is typical of a weakly crosslinked network in the rubbery state.

0

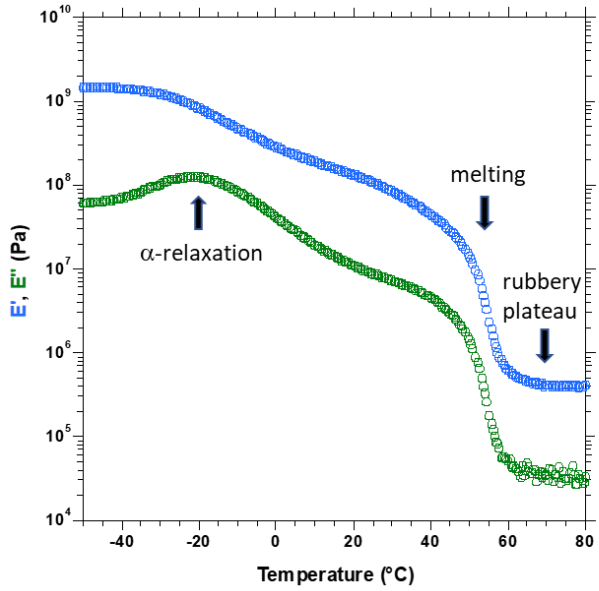


Figure 6: Plot of the storage and loss modulus (E', E'') of the polyester measured by DMTA

***Towards a model of the polyester network***

In our previous work on the polymerization of the crude fatty acid [7], we used Flory's theory of rubber elasticity [23] in order to estimate the crosslink density of the network from the E' modulus measured by DMTA at the rubbery plateau. The same approach can be applied to the polymer networks obtained in the present work by polymerization of the purified fatty acid. The crosslink density ν (mole.m$^{-3}$) is given by:

$$\nu = \frac{E}{3RT}$$

Where: R is the gaz constant 8.32 J.mol$^{-1}$.K$^{-1}$, T is the temperature in Kelvin and E the rubbery state elastic modulus at small deformation.

The modulus E' measured by DMTA at the rubbery plateau at 70°C (above the melting temperature) is equal to 0.4 MPa, which leads to a crosslink density of 47 mol.m$^{-3}$. This value is 16-fold lower than that of the networks obtained by polymerization of the crude fatty acid extract (728 mol.m$^{-3}$) [7], confirming that when present, the phenolic compounds significantly contribute to additional crosslinking reactions. The identification of such reactions may be the subject of future studies.

Figure 7 gives a model representation of the network formed by the polymerization of the purified CM extract. As indicated, "A" stands for an acid function and "B" for and hydroxyl function, that can react to form ester bonds, notated "AB". For the sake of clarity, only 2 types of building blocks are used: monoacidic monomers abbreviated ABB (standing for the main diOHC16 monomer, plus the 16-hydroxyhexadecanoic acid minor compounds), and dicarboxylic monomers abbreviated A-A (standing for both the 10-hydroxyhexadecanedioic acid and the hexadecanedioic acid monomers). The

proposed structure of the elastically active chains between crosslinks is based on the following data and assumptions:

• The content of ABB and A-A building blocks in the chains corresponds to the composition of the refined CM extract (Figure 1B), i.e. approximately 95% and 5%, respectively.

•The average molecular mass Mc (g.mol-1) of an elastically active chain can be estimated from the Flory model:

$$M_c = \frac{\rho}{\nu}$$

Assuming a density $\rho$= 1 g.cm$^3$, as a first approximation, this gives Mc ≈ 21.4 × 10$^3$ g.mol-1.

•The number of repeating units in the chain can be estimated by dividing Mc by the mass of a repeating unit: $M_0 \approx 270$ g.mol$^{-1}$ (corresponding to an ABB molecule, when A and B end functions are reacted). This gives ≈ 80 repeating units, i.e. ≈ 4 A-A and ≈ 76 ABB.

• Due to the low reactivity of the secondary $\alpha$-hydroxyl groups (Figure 3C) of ABB building blocks, the majority of the ester bonds are formed by reactions between acid groups and primary $\omega$-hydroxyl groups, leading to linear sequences. However, a significant fraction of the ester bonds involves secondary $\alpha$-hydroxyl groups, leading to side chains, and contributing to crosslinking by copolymerization with A-A building blocks.

Indeed, this proposed model highlights a key role of the minor dicarboxylic fatty acid compounds (A-A) in the formation of the three-dimensional network by connecting linear parts of branched chains. Figure 7 shows that the elastically active chains resulting from these connections are delimited by crosslinking nodes. Pendant chains are connected to the elastically active chain by simple branching points. In this structure, long linear sequences -ABBABBABBABBABB- are assumed to be able to pack as crystals (parallel packing of different elastically active chains), resulting in the semi-crystalline structure evidenced by X-Ray experiments.

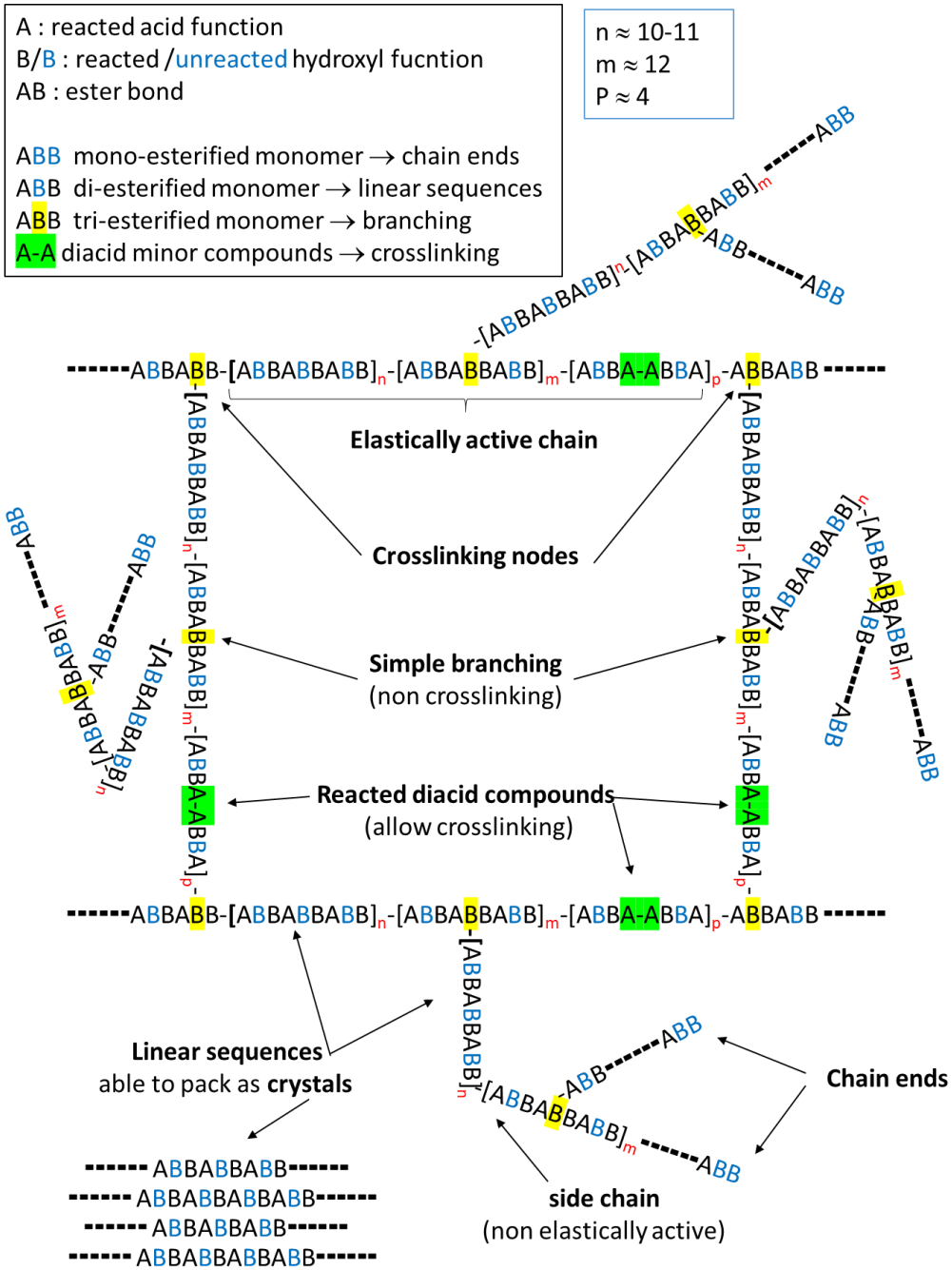


Figure 7: Model representation of the polyester network

***Mechanical properties exhibit a plastic deformation and necking phenomena***

Figure 8 shows a superposition of tensile stress–strain curves for the cross-linked polyester. The average mechanical properties are a Young's modulus of 72 MPa, a maximum strength of 8.2 MPa and an elongation at break of 286%. The superposition of the curves shows a good reproducibility in the mechanical behavior of the specimens. An elastic domain is observed until 25% strain where a maximum stress is measured at about 8 MPa. A flow threshold occurs at higher deformation accompanied by the formation of a distinct visible neck, a load drop in the stress-strain curve, and neck

propagation at constant stress of about 6 MPa. This corresponds to a plastic deformation until rupture. The necking corresponds to a deformation propagating at a constant rate along the axis of stretching [39]. Macroscopically the deformation is heterogeneous, the thickness of the sample decreases dramatically in a localized domain. Necking is rarely reported for bio-based polymers but is well known for synthetic polymers such polyethylene where it corresponds to the orientation of the polymer chains [40]. In this study, the X-ray scattering anisotropy, which presents diffraction spots on equatorial and polar position, is due to the orientation of the crystallized polyester particles parallel to the direction of the deformation. The isotropic X-ray scattering signal recorded before stretching of the polyester is due to the random arrangement of the polyester crystal particles, with the peak at 10 Å and the lateral packing of the chains recorded at wide angles. DSC measurements indicate the same crystal concentration before and after stretching the sample. This mechanical behavior of wide plastic deformation observed in the purified polyester is completely different from the elastomeric properties observed in the crude polyester [7]. The presence of a low level of crosslinks induces crystallinity that increases tensile strength. The extent of deformation is accompanied by a crystal orientation. Moreover, it has been observed that the heating at 75°C of the sample elongated before breaking, provokes the recovery of its initial length. It means that the deformation is thermally reversible allowing shape memory properties.

The mechanical and thermal properties are compared with those of some common polymers and biodegradable aliphatic polyesters in the supplementary table based on bibliographic data[41 42 43]. The mechanical properties of cutin polyester combined with its remarkable necking behavior during deformation, are comparable to those of LDPE. In terms of glass transition, the Tg of the polyester is in the same order of magnitude as that of other biodegradable polyesters such as PBS. On the other hand, the melting temperature of the crystal fraction remains low at 51°C but it should be noted that, at this temperature, there is no flow and the material retains its initial shape.

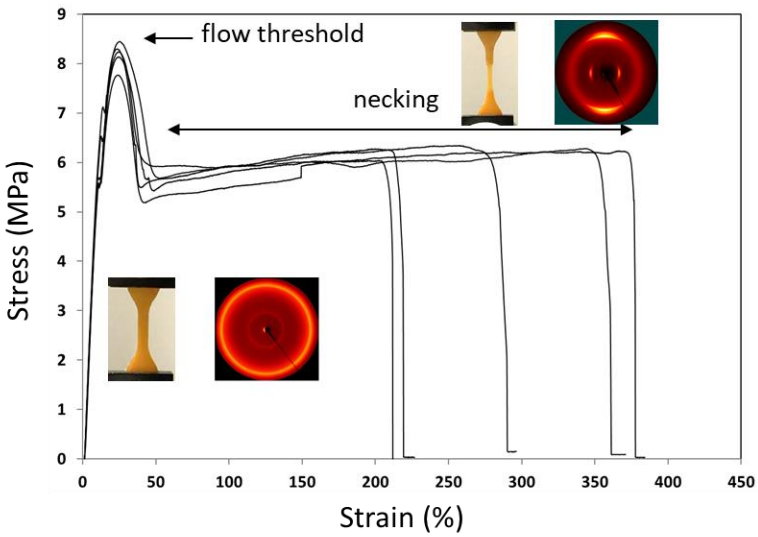


Figure 8: Stress-strain curves obtained on tensile of polyester. Inserted images show the initial dogbone shape of material and necking phenomena with a juxtaposition of two-dimensional WAXS diagrams.

***Shape memory properties are consistent with a crosslinked semi-crystalline structure***

The polyester material exhibited shape memory properties which seems logical given the slightly crosslinked semi-crystalline structure. Shape memory behavior of a polymer is the ability of a material to change its shape from a temporary to a permanent shape at a given temperature. To demonstrate this effect, a sample in the shape of ring, cut in the thick film (0.7 mm), was heated and stretched at 75°C, above the melting temperature of the polyester, and cooled rapidly to 10°C while maintaining this shape (Figure 9a). Later, the deformed sample was immersed in a water bath at 60°C (Figure 9b to 9e) and the deformed sample recovered its original shape in 2 seconds (Figure 9f).

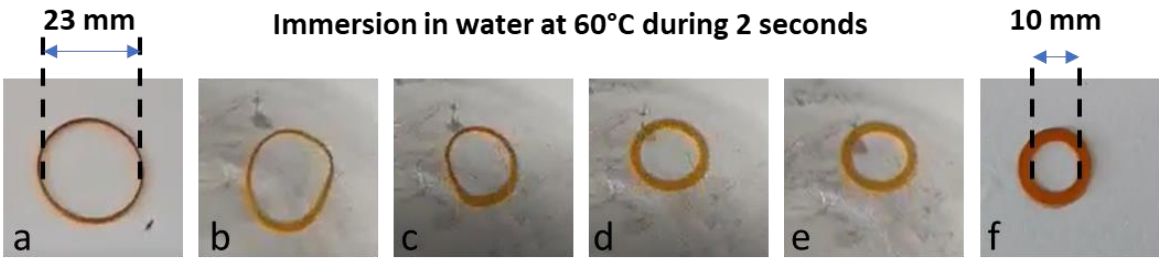


Figure 9: Shape recovery of a polyester ring immersed in water at 60°C

Shape recovery can be assessed by DMTA by measuring accurately the evolution of the sample length simultaneously with its modulus (Figure 10). The permanent shape is a small dogbone with an effective length of 3.6 mm. It was previously elongated at 75°C by 100% (7.2 mm length) and quenched at room temperature, in order to obtain the temporary shape. WAXS measurements have shown quite similar features as in the case of necking. The spots observed in the 2D diagram show a strong crystal orientation in the temporary shape in the direction of its deformation. During heating, the sample length recovery starts at 45-50°C, to reach 100% recovery at 70-75°C. Shape recovery is simultaneous with the melting of the crystal previously detected by DSC in the same temperature range. At the same time, the crystal orientation completely disappears as shown by WAXS after cooling. These results show a clear relationship between the slightly crosslinked semi-crystalline structure of the polymer and its shape memory behavior [44, 45]. The stretching of the polymer chains at a temperature higher than the melting temperature, allows their orientation, the presence of a reticulated network avoids the flowing of the polymer. Freezing under stress leads to oriented crystals in the direction of deformation. At room temperature the structure is maintained by crystals that allow the temporary shape stability. When the material is heated above the melting temperature of crystal domains, the permanent shape is spontaneously recovered driven by the reticulated elastic entropy of the extended and reticulated chains. Similar shape memory properties have been observed on dogbone elongated at room temperature and showing necking phenomena (result not shown). This observation makes it possible to envisage a cold programming of the shape memory

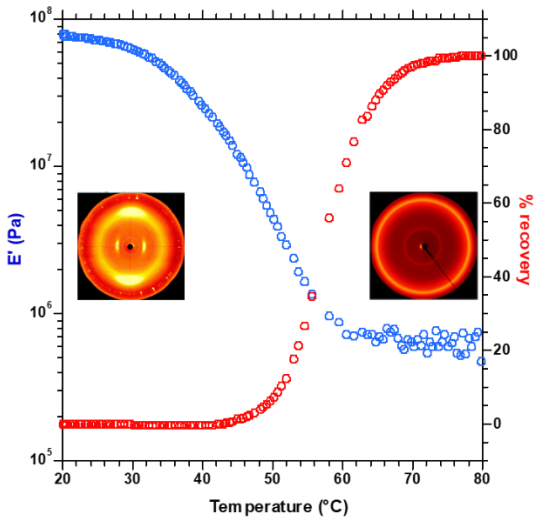


Figure 10: Storage modulus E' and percentage of recovery measured by DMTA during shape recovery of polyester with a juxtaposition of two-dimensional WAXS diagrams obtained after cooling.

It appears clearly that this shape memory behavior is related to the presence of long elastically active chains between the nodes of the network, that are able to crystallize. Therefore, it may be affected by variations of the phenolic and diacid impurities contents: For phenolics, the potential impact may be strong. However, we cannot predict it because we currently do not know the exact nature of the additional crosslinking reactions that they induce (Future works may elucidate this point). For diacid impurities, the potential impact can be inferred from the proposed model representation of the polyester network (Figure 7): Each additional diacid molecule in the initial reaction medium can potentially lead the formation of one additional elastically active chain by "bridging" two pendent chains. In other words, assuming that all diacid molecules participate in the formation of elastically active chains implies that the crosslink density is proportional to the diacid concentration. Calculations based on this assumption (detailed in supplementary material) lead to the conclusion that for a diacid concentration range $4 < x < 6$ %, the variations should be: $38 < \nu < 56$ mol/m3 for the crosslink density, and $26 > Mc > 18$ Kg/mol for the average mass of elastically active chains, which number of repetitive units should thus vary within the range $98 > Mc/M0 > 65$ units. We assume that such variations are unlikely to affect the ability of the elastically active chains to crystallize, and so the presence of a shape memory behavior. However, they should affect the crystallinity index and so the tensile mechanical properties at room temperature. The rubbery storage modulus above the melting temperature will of course also be affected (in the range $0.32 < E'(70°C) < 0.48$ MPa according to our calculations).

## Conclusions

A fully bio-based shape memory polyester was successfully synthesized without a catalyst, from a biorefined hydroxy fatty acid extract produced from tomato pomaces. As a proof-of-concept, this work demonstrates how monomer purification can drastically affects the functional properties of the polyester, and should be considered as a key parameter in the design of a cutin biorefinery process. Nevertheless, an up-scalable phenolic and eco-friendly removal process should be further developed to take advantage of the unique shape memory and mechanical properties of the polyester from an

industrial and commercial perspective. Indeed, while amorphous elastomers are produced from the crude hydroxy-fatty acid fraction of tomato peels, the purification step we developed, promotes the production of a semi-crystalline polyester with high mechanical and shape memory properties. By linking the linear parts of a branched structure dominated by the major diOHC16, the minor α, ω-hexadecanedioic acids of the hydroxy fatty acid fraction as well as H-bonds, a 3D network is formed that does not flow above the melting temperature. The linear parts of the chains are long enough to crystallize in large parts and control the mechanical properties at room temperature. The structure resulting from the combination of crystal and elastic network provides shape memory properties. In the future, it seems possible to optimize the mechanical and thermomechanical properties of bio-based polymers by controlling the level of minor components, first in the design of the biorefinery cascade or by valorizing other bio-sourced synthons. Indeed, our findings open a new path for the rational design of multifunctional polyester networks, enabling the future advancement of high-performance materials to meet the expectations of a circular economy of the agro-industrial food chain.

## Acknowledgment

SOLEIL synchrotron staff is acknowledged for selecting and allocating beamtime to the BAG 20211135 (Soft Matter applications: multi-scale structural studies of nanocomposites, colloidal complexes, gels and lipid assemblies) on the SWING beamline. Javier Pérez (group leader beamline SWING, SOLEIL synchrotron) is acknowledged for the set-up, and the GDR2019 CNRS/INRAE "Solliciter LA Matière Molle" (SLAMM) for partially funding the BAG. André Lelion, Anne-Lyse Panhéleux and Hyazann Hulin are acknowledged for their technical support.

## References

(1) Cywar, R. M.; Rorrer, N. A.; Hoyt, C. B.; Beckham, G. T.; Chen, E. Y. X. Bio-based polymers with performance-advantaged properties. *Nature Reviews Materials* **2022**, *7* (2), 83-103. DOI: https://doi.10.1038/s41578-021-00363-3.

(2) Queneau, Y.; Han, B. Biomass: renewable carbon resource for chemical and energy industry. *The Innovation* **2022**, *3* (1), 100184. DOI: https://doi.org/10.1016/j.xinn.2021.100184.

(3) Zhu, Y. Q.; Romain, C.; Williams, C. K. Sustainable polymers from renewable resources. *Nature* **2016**, *540* (7633), 354-362. DOI: https://10.1038/nature21001.

(4) Canevali, C.; Orlandi, M.; Pardi, L.; Rindone, B.; Scotti, R.; Sipila, J.; Morazzoni, F. Oxidative degradation of monomeric and dimeric phenylpropanoids: reactivity and mechanistic investigation. *Journal of the Chemical Society-Dalton Transactions* **2002**, (15), 3007-3014. DOI: https://10.1039/b203386k.

(5) Anastas, P. T.; Kirchhoff, M. M. Origins, Current Status, and Future Challenges of Green Chemistry. *Accounts of Chemical Research* **2002**, *35* (9), 686-694. DOI: https://10.1021/ar010065m.

(6) Duarah, P.; Haldar, D.; Purkait, M. K. Technological advancement in the synthesis and applications of lignin-based nanoparticles derived from agro-industrial waste residues: A review. *International Journal of Biological Macromolecules* **2020**, *163*, 1828-1843. DOI: https://10.1016/j.ijbiomac.2020.09.076.

(7) Marc, M.; Risani, R.; Desnoes, E.; Falourd, X.; Pontoire, B.; Rodrigues, R.; Escorcio, R.; Batista, A. P.; Valentin, R.; Gontard, N.; et al. Bioinspired co-polyesters of hydroxy-fatty acids extracted from tomato peel agro-wastes and glycerol with tunable mechanical, thermal and barrier properties. *Industrial Crops and Products* **2021**, *170*. DOI: https://10.1016/j.indcrop.2021.113718.

(8) Stempfle, F.; Ortmann, P.; Mecking, S. Long-chain aliphatic polymers to bridge the gap between semicrystalline polyolefins and traditional polycondensates. *Chemical Reviews* **2016**, *116* (7), 4597-4641. DOI: https://10.1021/acs.chemrev.5b00705.

(9) Wang, Z. K.; Ganewatta, M. S.; Tang, C. B. Sustainable polymers from biomass: Bridging chemistry with materials and processing. *Progress in Polymer Science* **2020**, *101*. DOI: https://10.1016/j.progpolymsci.2019.101197.

(10) Vilela, C.; Sousa, A. F.; Fonseca, A. C.; Serra, A. C.; Coelho, J. F. J.; Freire, C. S. R.; Silvestre, A. J. D. The quest for sustainable polyesters - insights into the future. *Polymer Chemistry* **2014**, *5* (9), 3119-3141. DOI: 10.1039/c3py01213a.

(11) Bakan, B.; Marion, D. Assembly of the Cutin Polyester: From Cells to Extracellular Cell Walls. *Plants (Basel)* **2017**, *6* (4). DOI: https://10.3390/plants6040057.

(12) Yeats, T. H.; Rose, J. K. C. The formation and function of plant cuticles. *Plant Physiology* **2013**, *163* (1), 5-20. DOI: https://10.1104/pp.113.222737.

(13) Benitez, J. J.; Castillo, P. M.; del Rio, J. C.; Leon-Camacho, M.; Dominguez, E.; Heredia, A.; Guzman-Puyol, S.; Athanassiou, A.; Heredia-Guerrero, J. A. Valorization of tomato processing by-products: fatty acid extraction and production of bio-based materials. *Materials* **2018**, *11* (11). DOI: https://10.3390/ma11112211.

(14) Gandini, A.; Pascoal Neto, C.; Silvestre, A. J. D. Suberin: A promising renewable resource for novel macromolecular materials. *Progress in Polymer Science* **2006**, *31* (10), 878-892. DOI: https://doi.org/10.1016/j.progpolymsci.2006.07.004.

(15) Vangeel, T.; Neiva, D. M.; Quilhó, T.; Costa, R. A.; Sousa, V.; Sels, B. F.; Pereira, H. Tree bark characterization envisioning an integrated use in a biorefinery. *Biomass Conversion and Biorefinery* **2023**, *13* (3), 2029-2043. DOI: 10.1007/s13399-021-01362-8.

(16) Heredia-Guerrero, J. A.; Heredia, A.; Dominguez, E.; Cingolani, R.; Bayer, I. S.; Athanassiou, A.; Benitez, J. J. Cutin from agro-waste as a raw material for the production of bioplastics. *Journal of Experimental Botany* **2017**, *68* (19), 5401-5410. DOI: https://10.1093/jxb/erx272.

(17) Casa, M.; Miccio, M.; De Feo, G.; Paulillo, A.; Chirone, R.; Paulillo, D.; Lettieri, P.; Chirone, R. A brief overview on valorization of industrial tomato by-products using the biorefinery cascade. *Detritus* **2021**, *15*, 31-39. DOI: https://10.31025/2611-4135/2021.14088.

(18) Escorcio, R.; Bento, A.; Tome, A. S.; Correia, V. G.; Rodrigues, R.; Moreira, C. J. S.; Marion, D.; Bakan, B.; Silva Pereira, C. Finding a Needle in a Haystack: Producing Antimicrobial Cutin-Derived Oligomers from Tomato Pomace. *ACS Sustain Chem Eng* **2022**, *10* (34), 11415-11427. DOI: https://10.1021/acssuschemeng.2c03437.

(19) Lu, Z. Q.; Wang, J. J.; Gao, R. P.; Ye, F. Y.; Zhao, G. H. Sustainable valorisation of tomato pomace: A comprehensive review. *Trends in Food Science & Technology* **2019**, *86*, 172-187. DOI: https://10.1016/j.tifs.2019.02.020.

(20) Cogognigni, I.; Montanari, A.; de la, T. C., R., ; Cardoso Bernet Montserrat, G. Extraction method of a polyester polymer or cutin from the wasted tomato peels and polyester polimer so extracted. WO-2015028299-A1, 2014.

(21) Montanari, A.; Bolzoni, L.; Cigognini, I. M.; Ciruelos, A.; Cardoso, M. G.; de la Torre, R. Tomato bio-based lacquer for sustainable metal packaging. *Acta Horticulturae* **2016**, *1159*, 159-166. DOI: https://10.17660/ActaHortic.2017.1159.24.

(22) Tedeschi, G.; Benitez, J. J.; Ceseracciu, L.; Dastmalchi, K.; Itin, B.; Stark, R. E.; Heredia, A.; Athanassiou, A.; Heredia-Guerrero, J. A. Sustainable fabrication of plant cuticle-like packaging films from tomato pomace agro-waste, beeswax, and alginate. *Acs Sustainable Chemistry & Engineering* **2018**, *6* (11), 14955-14966. DOI: https://10.1021/acssuschemeng.8b03450.

(23) Flory, P. J. Molecular Size Distribution in Three Dimensional Polymers. VI. Branched Polymers Containing A—R—Bf-1 Type Units. *Journal of the American Chemical Society* **1952**, *74* (11), 2718-2723. DOI: https://doi.org/10.1021/ja01131a008.

(24) Zamora, R.; Hidalgo, F. J. The triple defensive barrier of phenolic compounds against the lipid oxidation-induced damage in food products. *Trends in Food Science & Technology* **2016**, *54*, 165-174. DOI: https://doi.org/10.1016/j.tifs.2016.06.006.
(25) Honda, S.; Ishida, R.; Hidaka, K.; Masuda, T. Stability of polyphenols under alkaline conditions and the formation of a xanthine oxidase inhibitor from gallic acid in a solution at pH 7.4. *Food Science and Technology Research* **2019**, *25* (1), 123-129. DOI: https://10.3136/fstr.25.123.
(26) Kaluzny, M. A.; Duncan, L. A.; Merritt, M. V.; Epps, D. E. Rapid separation of lipid classes in high yield and purity using bonded phase columns. *J Lipid Res* **1985**, *26* (1), 135-140. DOI: https://doi.org/10.1016/S0022-2275(20)34412-6 From NLM.
(27) Singleton, V. L.; Orthofer, R.; Lamuela-Raventós, R. M. Analysis of total phenols and other oxidation substrates and antioxidants by means of folin-ciocalteu reagent. In *Methods in Enzymology*, Vol. 299; Academic Press, 1999; pp 152-178.
(28) Robbins, R. J.; Bean, S. R. Development of a quantitative high-performance liquid chromatography–photodiode array detection measurement system for phenolic acids. *Journal of chromatography A* **2004**, *1038* (1-2), 97-105.
(29) Girard, A. L.; Mounet, F.; Lemaire-Chamley, M.; Gaillard, C.; Elmorjani, K.; Vivancos, J.; Runavot, J. L.; Quemener, B.; Petit, J.; Germain, V.; et al. Tomato GDSL1 is required for cutin deposition in the fruit cuticle. *Plant Cell* **2012**, *24* (7), 3119-3134. DOI: https://10.1105/tpc.112.101055.
(30) Velickovic, D.; Herdier, H.; Philippe, G.; Marion, D.; Rogniaux, H.; Bakan, B. Matrix-assisted laser desorption/ionization mass spectrometry imaging: a powerful tool for probing the molecular topology of plant cutin polymer. *Plant J* **2014**, *80* (5), 926-935. DOI: https://10.1111/tpj.12689.
(31) Philippe, G.; Gaillard, C.; Petit, J.; Geneix, N.; Dalgalarrondo, M.; Bres, C.; Mauxion, J. P.; Franke, R.; Rothan, C.; Schreiber, L.; et al. Ester Cross-Link Profiling of the Cutin Polymer of Wild-Type and Cutin Synthase Tomato Mutants Highlights Different Mechanisms of Polymerization. *Plant Physiol* **2016**, *170* (2), 807-820. DOI: https://10.1104/pp.15.01620.
(32) Wojdyr, M. Fityk: a general-purpose peak fitting program. *Journal of Applied Crystallography* **2010**, *43* (5 Part 1), 1126-1128. DOI: doi:10.1107/S0021889810030499.
(33) Heredia-Guerrero, J. A.; Benitez, J. J.; Dominguez, E.; Bayer, I. S.; Cingolani, R.; Athanassiou, A.; Heredia, A. Infrared and Raman spectroscopic features of plant cuticles: a review. *Front Plant Sci* **2014**, *5*, 305. DOI: https://10.3389/fpls.2014.00305.
(34) Hübner, W.; Blume, A. Interactions at the lipid–water interface. *Chemistry and Physics of Lipids* **1998**, *96* (1), 99-123. DOI: https://doi.org/10.1016/S0009-3084(98)00083-8.
(35) Žagar, E.; Grdadolnik, J. An infrared spectroscopic study of H-bond network in hyperbranched polyester polyol. *Journal of Molecular Structure* **2003**, *658* (3), 143-152. DOI: https://doi.org/10.1016/S0022-2860(03)00286-2.
(36) Bellamy, L. J. *The Infrared Spectra of Complex Molecules*; Chapman and Hall, 1975. DOI: https://10.1007/978-94-011-6017-9.
(37) Chaudhari, S. A.; Singhal, R. S. Cutin from watermelon peels: A novel inducer for cutinase production and its physicochemical characterization. *International Journal of Biological Macromolecules* **2015**, *79*, 398-404. DOI: https://doi.org/10.1016/j.ijbiomac.2015.05.006.
(38) Small, D. M. Handbook of Lipid Research: The Physical Chemistry of Lipids: From Alkanes to Phospholipids. In *In Handbook of Lipid Research*, Vol. 4; 1986.
(39) Neale, K. W.; Tuğcu, P. Analysis of necking and neck propagation in polymeric materials†. *Journal of the Mechanics and Physics of Solids* **1985**, *33* (4), 323-337. DOI: https://doi.org/10.1016/0022-5096(85)90032-8.
(40) Li, H.; Zhou, W.; Ji, Y.; Hong, Z.; Miao, B.; Li, X.; Zhang, J.; Qi, Z.; Wang, X.; Li, L.; Li, Z.-M. Spatial distribution of crystal orientation in neck propagation: An in-situ microscopic infrared imaging study on polyethylene. *Polymer* **2013**, *54* (2), 972-979. DOI: https://doi.org/10.1016/j.polymer.2012.12.012.
(41) Luzi, F.; Torre, L.; Kenny, J. M.; Puglia, D. Bio- and Fossil-Based Polymeric Blends and Nanocomposites for Packaging: Structure–Property Relationship. *Materials* **2019**, *12* (3), 471.

(42) Naser, A. Z.; Deiab, I.; Darras, B. M. Poly(lactic acid) (PLA) and polyhydroxyalkanoates (PHAs), green alternatives to petroleum-based plastics: a review. *RSC Advances* **2021**, *11* (28), 17151-17196, 10.1039/D1RA02390J. DOI: 10.1039/D1RA02390J.
(43) Xu, J.; Guo, B. H. Microbial Succinic Acid, Its Polymer Poly(butylene succinate), and Applications. In *PLASTICS FROM BACTERIA: NATURAL FUNCTIONS AND APPLICATIONS*, Chen, G. Q. Ed.; Vol. 14; 2010; pp 347-388.
(44) Behl, M.; Lendlein, A. Shape-memory polymers. *Materials Today* **2007**, *10* (4), 20-28. DOI: https://doi.org/10.1016/S1369-7021(07)70047-0.
(45) Zhao, Q.; Qi, H. J.; Xie, T. Recent progress in shape memory polymer: New behavior, enabling materials, and mechanistic understanding. *Progress in Polymer Science* **2015**, *49*, 79-120. DOI: https://doi.org/10.1016/j.progpolymsci.2015.04.001.

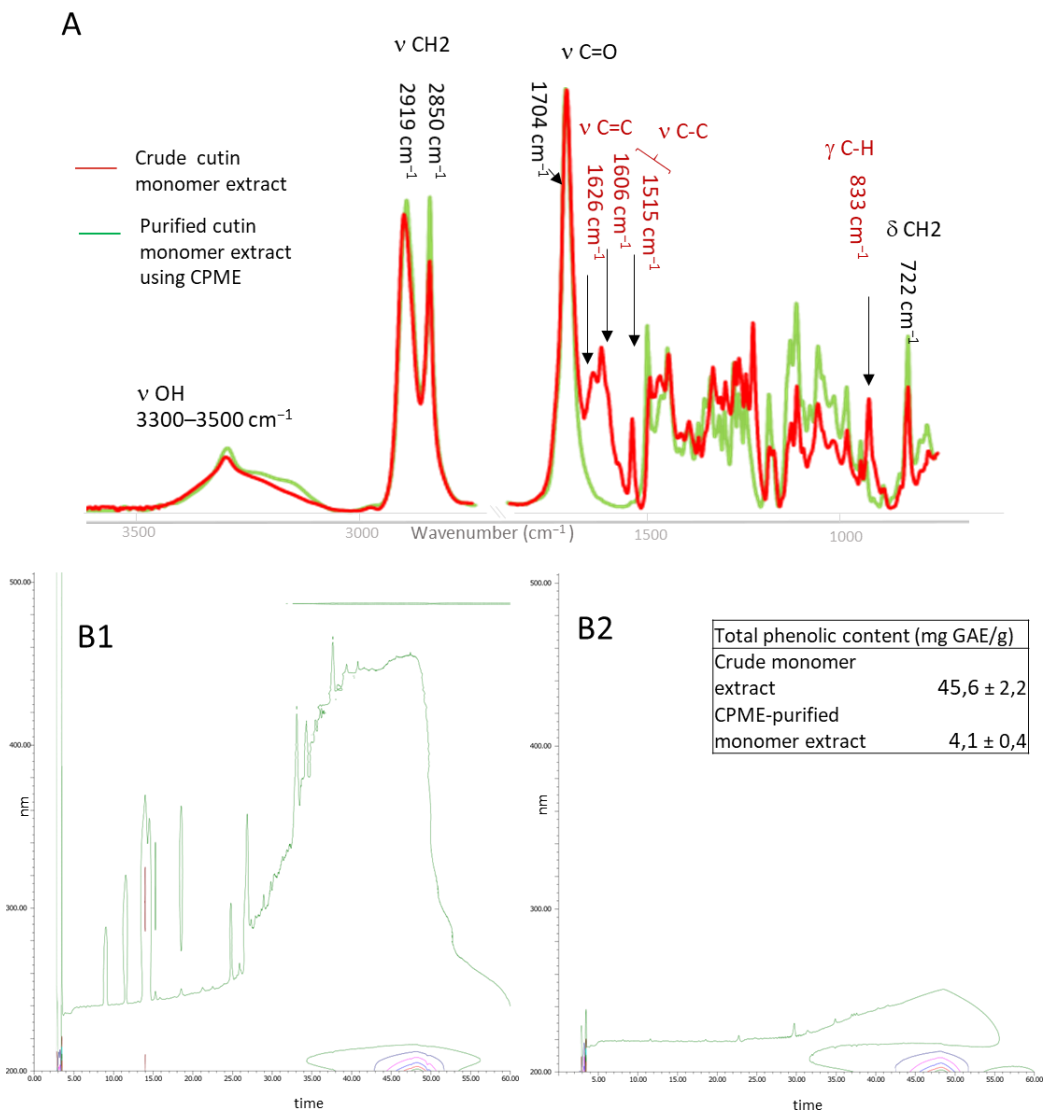


Supplemental figure 1: Characterization of the cutin monomers extracts before and after purification using green solvent.

The same conditions of purification of the cutin monomer were used, except that the chloroform was replaced by cyclopentyl methyl ether (CPME) and a washing step of the column with Acetone was added before elution.

(A) FT-IR analyses. Spectra are dominated by intense stretching vibrations of the methylene chains (asymmetric (CH2) and symmetric (CH2) at 2919 cm−1, and 2850 cm−1 respectively, bending CH2 at 722 cm−1) and a sharp band at 1704 cm−1 assigned to carbonyl stretch of carboxylic acid. A broad hydroxyl (3300–3500 cm−1) band was also observed. All these features are typical signatures of hydroxy fatty acids. The purification step led to the reduction of phenolic specific bands (red arrows) at 1626 cm-1 (stretching of conjugated C=C in aromatics), 1606 cm-1 (stretching band (C-C) aromatic ), 1515 cm-1 (stretching of C-C aromatic conjugated with C=C) and 833 cm-1 (out of plane bending of (C-H) aromatic).

Phenolic content determined by Folin Calieu analysis (inset- data expressed as mg of equivalent gallic acid per g of cutin extract) and by HPLC-DAD. Contour plot of the crude cutin monomer extract (B1) and CPME-purified cutin monomer (B2).

708

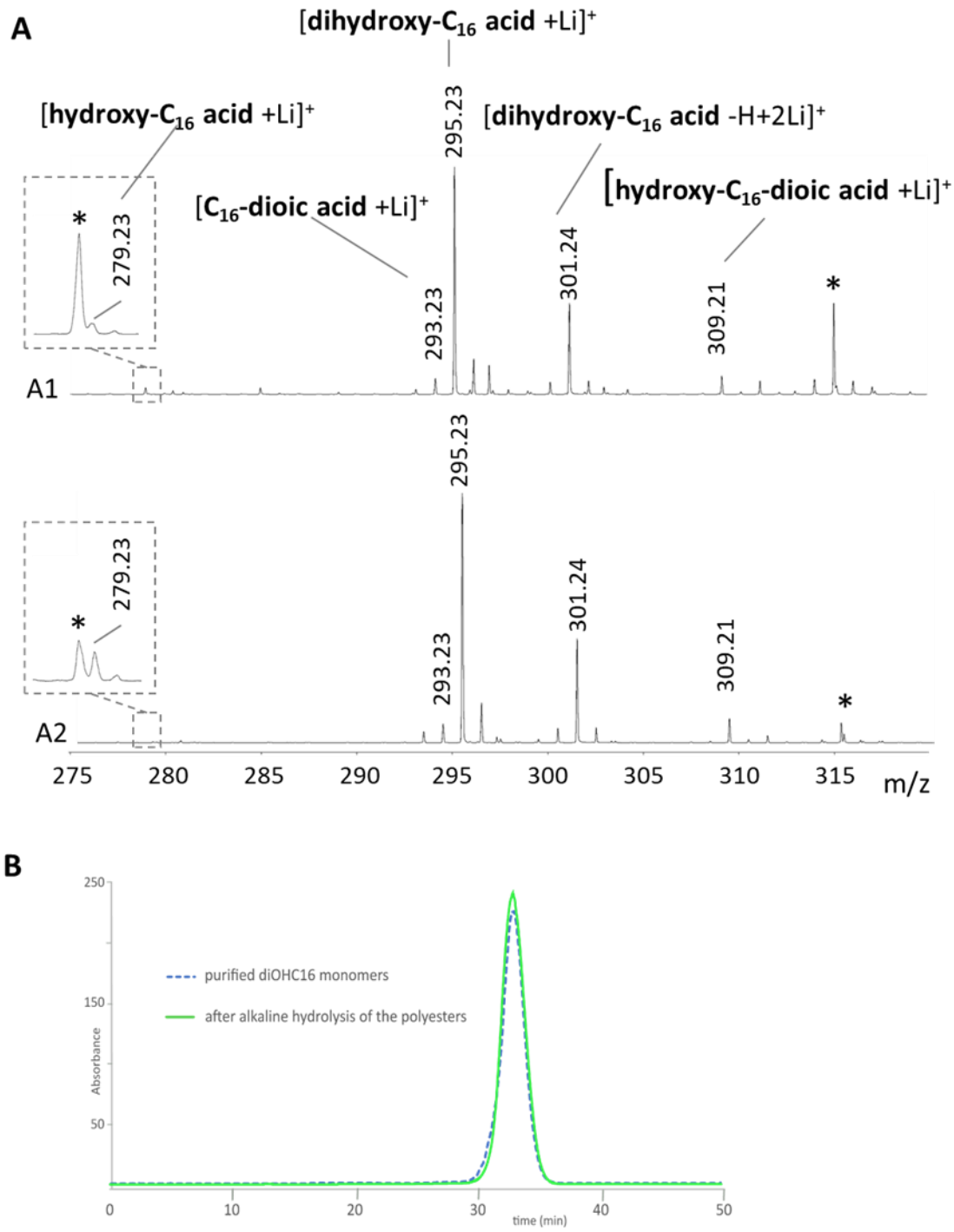


709

710

711 Supplemental Figure 2: Alkaline hydrolysis of the polymer.

712 A. MALDI-MS(+) spectra of the purified cutin monomers used for the polyester synthesis (A1) and after
713 alkaline hydrolysis of the polyester (A2). Annotations were deduced from exact mass measurements
714 in the range 275-320 Da. Black star indicates an ion from the MALDI matrix. B. Size Exclusion
715 chromatography of the purified diOHC16 monomers before polymer synthesis and after polyester
716 alkaline hydrolysis.

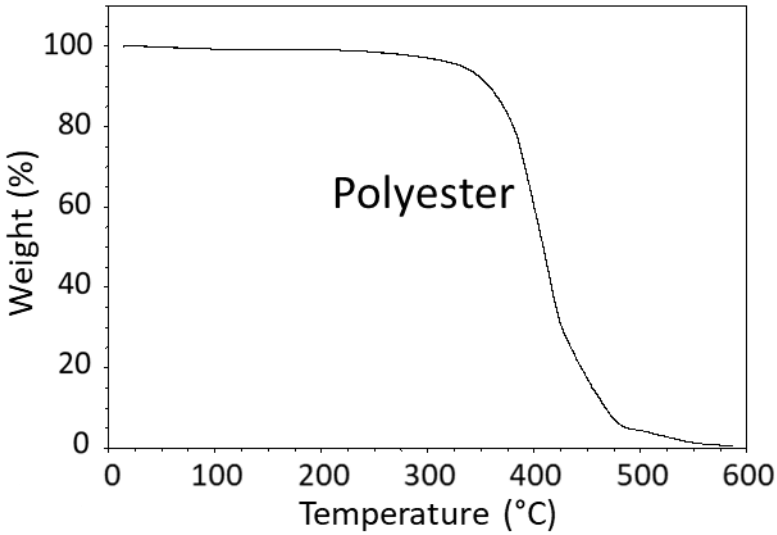


Supplemental Figure 3: Thermogravimetric analysis traces of the polyester

| | Tg (°C) | Tm (°C) | Tensile strenght (MPa) | Elongation at break (%) | ref |
|---|---|---|---|---|---|
| PET | 70-87 | 243-268 | 48-72 | 20-300 | 41 |
| HDPE | -125 to -90 | 135 | 22-31 | 100 to >1000 | 41 |
| LDPE | -125 to -100 | 112-135 | 8-31 | 200-900 | 41 |
| PP | -10 | 167-177 | 31-41 | 100-600 | 41 |
| PCL | -60 to -65 | 150-162 | 20-42 | 300-1000 | 42 |
| PHB | 5-15 | 168-182 | 40 | 5-8 | 42 |
| PHBV | -1 | 136-162 | 30-38 | 20 | 42 |
| PHBHHX | -1 | 127 | 21 | 400 | 42 |
| PBS | -32 | 114 | 34 | 560 | 43 |
| Cutin polyester | -25 | 51 | 8.2 | 286 | |

Supplemental table : Mechanical and thermal properties of common polymers and biodegradable aliphatic and semi-crystalline polyester, in comparison with cutin polyester

Estimation of the potential impact of diacid impurities content variations:

As explained in the text of the article, our calculations are based on the assumption that the crosslink density is proportional to the diacid concentration. Since the current x=5% leads to a crosslink density of 47 mol/m$^3$ a variation $\Delta$x (%) can potentially lead to a crosslink density:

$$\nu(\Delta x) = \frac{47}{5} \times (5 + \Delta x)$$

Therefore, for a range of variation of +/- 1% of diacid, We can expect the following values for crosslink density and related properties:

| Diacid % | Crosslink density<br>$\nu$ (mol/m$^3$) | Average mass between network nodes<br>$M_c$ (kg/mol) | Average number of repetitive units<br>$M_c/M_0$ | Rubbery modulus above melting temp.<br>E'(70°C) MPa |
|---|---|---|---|---|
| 4 | 38 | 26 | 98 | 0.32 |
| **5** | **47** | **21** | **79** | **0.4** |
| 6 | 56 | 18 | 65 | 0.48 |

The variations of the average mass and number of repeat units in elastically active chains are estimated assuming a density $\rho$= 1 g.cm$^3$, and a repetitive unit mass $M_0 \approx 270$ g.mol$^{-1}$. The model of Flory is used to calculate the corresponding rubbery storage modulus values.